JOURNAL OF GEOPHYSICAL RESEARCH, VOL. 95, NO. C2, PAGES 1741–1755, FEBRUARY 15, 1990

Ice Drift and Momentum Exchange in Winter Antarctic Pack Ice

DOUGLAS G. MARTINSON

Lamont-Doherty Geological Observatory and Department of Geological Sciences, Columbia University, Palisades, New York

CHRISTIAN WAMSER

Alfred-Wegener Institut für Polar und Meeresforschung, Bremerhaven, Federal Republic of Germany

This paper uses the Winter Weddell Sea Project 1986, winter Antarctic data set to (1) describe the nature of observed sea ice drift and momentum exchange and (2) determine relevant drag coefficients (linear and quadratic) and parameter values for three formulations of the momentum balance. The large-scale mean divergence of the ice justifies, with some penalty, use of the steady free drift equation in which the air-ice stress is balanced by ice-ocean drag and the Coriolis force. Three forms of the free drift equation are considered: (1) stresses are parameterized with a quadratic drag law, (2) stresses are parameterized with a linear drag law (useful because of its analytically manageable form), and (3) the Coriolis force is ignored (owing to the thin, 0.6-m ice), so ice speed is proportional to wind speed at a specified angle. All three formulations simulate the observed ice drift with the same degree of accuracy. The linear drag law is an excellent approximation to the quadratic law over a broad range of forcing only when the air-ice and ice-water stresses are both parameterized using the linear law (otherwise the ice-water drag coefficient is a nonconstant function of wind speed). The linear drag coefficient and constant of proportionality relating ice speed to wind speed can both be computed directly from knowledge of the quadratic values. These calculations result in estimates within $\lesssim$2% of the optimum fitted values. Because of the ~95% ice coverage, ice interaction is frequently significant. During such periods, the ice-water drag coefficient represents an "effective" drag, artificially inflated to include the forces arising from this interaction. We break the ice drift data into 6-hour nonoverlapping windows to allow isolation of periods of true free drift. Both true drag coefficient values and effective values are then estimated. The effective values show a strong correlation to the 4-day average large-scale ice divergence. They also show that the ice-water stress is typically ~1/3 the air-ice stress, indicating a significant role of ice interaction (free drift still provides an excellent parameterization of ice drift but at the expense of neglecting the details of these physics). The optimum quadratic drag coefficient is 1.62×10^{-3} with turning angle 15.2°; the effective value is 3.22×10^{-3} with turning angle 18.1°; the linear drag coefficient is 0.80×10^{-3} with turning angle 18.1°; the effective value is 1.48×10^{-3} with turning angle 19.6°, and in general, the ice drifts at ~3% of the wind speed, ~23° to its left.

1. INTRODUCTION

The study of pack ice drift has been shown, through previous studies, to be an effective tool for extracting information about surface velocities and stresses [e.g., *Rossby and Montgomery*, 1935; *McPhee*, 1979; *Feldman et al.*, 1981; *Thorndike and Colony*, 1982]. These studies, predominantly associated with the Arctic Ice Dynamics Joint Experiment (AIDJEX) and Marginal Ice Zone Experiment (MIZEX) programs in the Arctic, served to define and advance our understanding of the nature of momentum exchange between the atmosphere and ocean in the presence of a sea-ice cover. They have also provided estimates of characteristic values, under a variety of environmental conditions, for relevant parameters necessary to model this exchange. At present, no such estimates exist for Antarctic conditions except for those of *Rossby and Montgomery* [1935], which used the historical data set from the *Deutschland* during her entrapment in the (convergent) western Weddell in 1911 [*Brennecke*, 1921].

In general, conditions in the Antarctic are different from those of the Arctic, and while the fundamental physics governing momentum exchange are essentially independent of environmental specifics, the parameter values and modeling approaches are not. In the Antarctic, periods of free drift, when the internal ice stress is negligible and the ice momentum balance greatly simplified, may be more common throughout the ice season and spatially widespread given the mean divergent winds and lack of physical boundaries in the predominant drift directions. Also, most Antarctic pack ice is seasonal and remarkably thin ($\lesssim$60 cm; *Wadhams et al.* [1987]), minimizing the role of the Coriolis force in the momentum balance and possibly influencing the nature of internal ice stresses relative to those in the thicker multiyear ice of the Arctic. Further, while ice ridging can attain Arctic spatial frequencies, the ridge amplitudes are usually smaller. This combined with the potential for frequent underside melting due to the tremendous reservoir of ocean heat near the surface may lead to ice which is smoother than typical Arctic ice. Other differences may arise from the marginal stability of the Antarctic surface waters which leads to deep winter mixed layers. These deep mixed layers can moderate the amplitude of the ocean's inertial cycles, reduce the likelihood or magnitude of momentum dissipation through internal wave generation, and influence the characteristics of the oceanic planetary boundary layer (OBL) in general. These differences reflect the need to estimate relevant momentum exchange parameters directly within Antarctic conditions.

Paper number 89JC02958.
0148-0227/90/89JC-02958$05.00

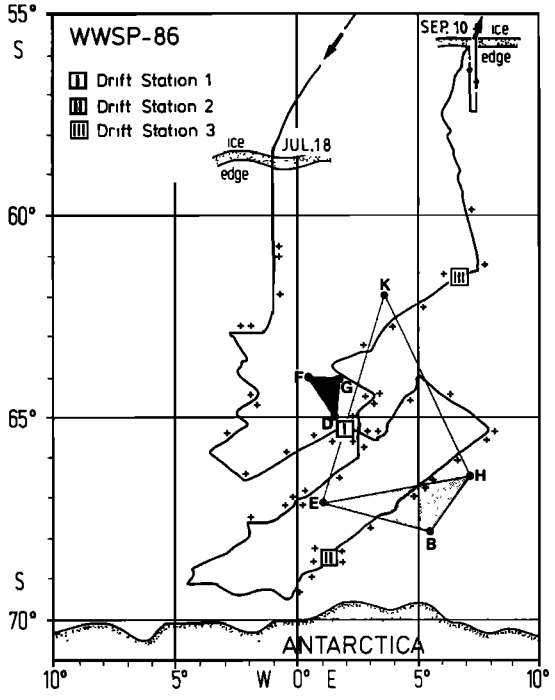

Fig. 1. Cruise track for the first leg of the Winter Weddell Sea Project, 1986. Three 4- to 5-day drift stations are shown by labeled boxes. Locations of air-ice stress measurements are indicated by small crosses. Large dots indicate mid-August location of ice-locked buoys which encompass triangular areas (shaded) used to estimate large-scale ice divergence.

In the austral winter of 1986, a detailed investigation within the Antarctic sea-ice cover along the eastern margin of the Weddell Sea was conducted during the first leg of the Winter Weddell Sea Project (WWSP-86) onboard the RV *Polarstern*. This leg concentrated on physical measurements along a cruise track (Figure 1) which covered the region between 5°W and 10°E from the ice margin, near 59°S, to the Antarctic continent. During this period, detailed measurements of the ocean, sea-ice, and atmosphere were made, providing the first extensive data set describing winter conditions within the Antarctic seasonal sea-ice field. Included with these data are observations made during three 4- to 5-day drift stations (Figure 1) as well as those from meteorological and oceanographic ice-locked Argos buoys [*Hoeber and Gube-Lehnhardt*, 1987] deployed along the cruise track. This paper uses these data to (1) describe the nature of the observed ice drift and momentum exchange and (2) determine relevant drag coefficients (linear and quadratic) and parameter values for several useful formulations of the ice momentum balance best suited to describe these observations.

2. Momentum Balance

A brief review of the momentum balance is presented here to define parameters and clearly present the assumptions, limitations, and practical aspects of the formulations for which parameter estimates are required. Throughout, a bold face variable indicates a complex quantity (two-dimensional horizontal vector). The velocity vector $\mathbf{V} = u + iv$ has horizontal velocity components u and v, pointing to the east

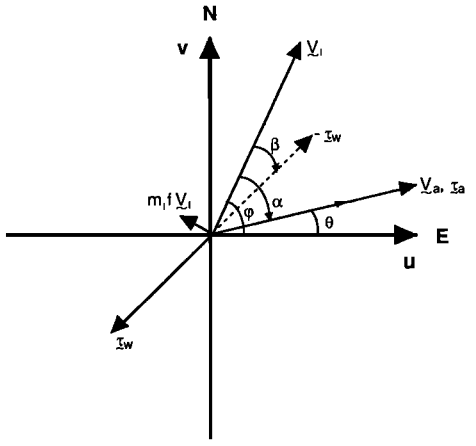

Fig. 2. Schematic of force vectors for free drift momentum balance formulation with associated notation (vectors are not scaled relative). The angles β and δ are positive when rotated clockwise. The air-ice stress is assumed to parallel the wind vector.

(positive x) and north (positive y) directions, respectively, and $i = (-1)^{1/2}$.

The conservation of momentum for ice can be written

$$m_i \frac{\partial \mathbf{V}_i}{\partial t} = -im_i f \mathbf{V}_i + \rho_a \boldsymbol{\tau}_a - \rho_w \boldsymbol{\tau}_w - \mathbf{I} \qquad (1)$$

where the ice mass per unit area $m_i = \rho_i \bar{h}_i$ (540 kg/m^2) with density ρ_i (900 kg/m^3) and average ice thickness $\bar{h}_i$ (0.6 m; *Wadhams et al.* [1987]), t is time, f is the Coriolis parameter (at 65°S, -1.32×10^{-4} s^{-1}), ρ_a (1.25 kg/m^3) and ρ_w (10^3 kg/m^3) are air and water densities, respectively, $\boldsymbol{\tau}_a$ and $\boldsymbol{\tau}_w$ are the vertical components of tangential kinematic stress vectors between air-ice and ice-water, respectively, and $\mathbf{I}$ is a residual force vector, predominantly associated with gradients of internal ice stress. The ice drift velocity is written relative to the geostrophic flow of the ocean ($\mathbf{V}_g$), and $\partial \mathbf{V}_g/\partial t$ is assumed small over the time scales of interest and neglected. Partial derivatives indicate a Lagrangian reference frame (with respect to $\mathbf{V}_g$). The sign convention is chosen to reflect that the air-ice stress is the momentum source, while the other terms act as momentum sinks. The change in ice mass with time ($\mathbf{V}_i\, \partial m_i/\partial t$) is ignored, since the slow winter growth rate, ~4 mm/d due to thermodynamics and a similar or smaller average rate due to ice rafting [*Wadhams et al.*, 1987], leads to an influence of <1% relative to the other terms in the balance.

The complex vectors for velocities and ice-water stress (the air-ice stress is assumed parallel to the wind) are written in polar form as (see Figure 2)

$$\mathbf{V}_i = |\mathbf{V}_i| e^{i\varphi}$$

$$\mathbf{V}_a = |\mathbf{V}_a| e^{i\theta} = |\mathbf{V}_a| e^{i(\varphi - \delta)}$$

$$\boldsymbol{\tau}_w = |\boldsymbol{\tau}_w| e^{i(\varphi - \beta)}$$

Direct measurements of stress are difficult to obtain, so stress is often formulated in terms of external parameters that are more easily measured. For stress magnitude, modern knowledge of the planetary boundary layer (PBL) structure suggests a power law of the form $|\boldsymbol{\tau}| = c_D |\mathbf{V}|^p$, where typically $1 \leq p \lesssim 2$ (powers >2 are sometimes required) and

c_D is a drag coefficient (c_a is air-ice drag and c_w is ice-water drag). Where direct stress measurements are available, the power and drag coefficient are determined directly from the measurements. Otherwise, the value of p is specified based upon some a priori knowledge or assumption concerning the specific structure of the PBL. Two limiting cases are most frequently employed: the linear and quadratic power laws. The former is consistent with a pure Ekman boundary layer, and the latter with a more realistic, though still idealistic, two-layer boundary (constant stress layer overlying the outer, Ekman, layer). The quadratic law is thus more consistent with theory and appears to be more representative of the observations in general [*McPhee*, 1980]. However, the linear drag law offers a significant advantage in its simpler, analytically manageable form and can represent a reasonable approximation to the quadratic law over typical ranges in **V**. This makes the linear drag law often preferable for simple modeling studies or those in which a detailed model analysis is desired. (Note that *McPhee* [1979] finds that Arctic OBL observations are actually best fit by $p = 1.78$, which is consistent with his theoretical predictions based upon a Rossby similarity scaling of the PBL equations.)

We simplify (1) by considering the linear and quadratic power laws. In addition, the WWSP-86 data are insufficient to resolve the nature of **I**, while time dependency appears to be negligible. Consequently, we ignore these terms and work directly with the free drift equation:

$$\rho_a|\tau_a|e^{-i\delta} = im_i f|\mathbf{V}_i| + \rho_w|\tau_w|e^{-i\beta} \qquad (2)$$

here rotated through an angle φ, so that $\mathbf{V}_i$ is parallel to the x axis.

The implications of ignoring the time dependence term are revealed by considering the time scales of its influence. In an ideal case where surface OBL velocities (e.g., inertial cycles) are small in magnitude relative to ice motion (i.e., $|\mathbf{V}_{PBL}| \ll |\mathbf{V}_i|$) and **I** is negligible, a linear power law for the ice-ocean stress allows an analytic solution to (1). This solution, an exponentially damped inertial cycle modifying a steady drift, has a relaxation time of $\lambda = m_i/(\rho_w c_w^1 \cos\beta)$, where c_w^1 is the linear drag coefficient. For typical Arctic ice thickness (3 m) and $c_w^1 = 8.6 \times 10^{-4}$ m/s [*McPhee*, 1980], $\lambda \sim 0.9$ hours, or steady state is achieved in ~3 hours. For the thinner Antarctic ice (0.6 m), $\lambda \sim 0.2$ hours for the same c_w^1, so steady state is achieved within an hour of any change in the external forcing. These short relaxation times hold for a wide range of c_w^1 values.

While this solution is for an overly simplified system, it qualitatively suggests that the ice itself is capable of achieving steady state rapidly following a change in the winds. However, the requirement $|\mathbf{V}_{PBL}| \ll |\mathbf{V}_i|$ is inconsistent with the findings of *McPhee* [1978], who found that the inertial motion is strongly concentrated near the surface of the OBL and in turn reflects inertial cycles in the ice drift. Therefore the time dependency of (1) is limited by the longest time scales of the OBL or the inertial period, ~12 hours.

Use of a power law, however, limits the time dependence of (1) to temporal scales which are long relative to transient time scales of the OBL, since the power law is derived from the PBL equations under the assumption of steady state conditions. This is also clearly demonstrated by *McPhee* [1978]. Thus consideration of time dependency is not required for time scales longer than those of the OBL transient behavior, and the power law parameterizations render the formulation incapable of describing the behavior during these shorter transient time scales. This suggests neglecting the time dependency and smoothing the data over inertial periods. In the winter months though, inertial motion is rarely observed in the Arctic and is absent from the WWSP-86 data as well. *McPhee* [1980] suggests that this is due to damping from ice interaction induced by the phase mismatch between nearby interacting inertial cycles in a relatively compact ice field. Further, the winds observed during WWSP-86 show spectral power concentrated in periods longer than several hours. So, the need for smoothing is essentially eliminated, since transient behavior is both short lived and infrequently generated. Neglect of the time dependence appears well justified.

For **I**, the mean divergence of most of the Antarctic ice field and lack of physical boundaries in the predominant drift directions suggest that neglect of this term is justified. However, additional observations suggest otherwise: (1) ice ridges are clearly evident throughout the winter Antarctic pack ice, (2) the WWSP-86 data (see next section) reveal frequent, though short-lived, periods of ice convergence superimposed on the mean divergence, (3) ~95% ice concentration suggests random ice bumping, and (4) absence of inertial motion implies local ice interaction. Ignoring **I** during periods in which ice interaction is significant, though not dominant, as is likely for much of the divergent Antarctic region, forces this unmodeled momentum loss to be artificially subsumed by the ice-ocean drag term. Consequently, during such periods, c_w and β represent "effective" values in the free drift equation. The physics of this treatment are inaccurate, and results sensitive to $\mathbf{V}_a$ and its variance because of the nonlinear nature of **I** [*Hibler*, 1986]. However, such values do allow an estimate of the ice drift and momentum exchange into the ocean which are still useful for numerous modeling purposes. Conversely, during periods of strong divergence, **I** is minimal, and use of the free drift equation should provide upper limit estimates for the true drag coefficient values representative of the steady OBL. We estimate both effective and true parameter values.

Finally, for typical Antarctic ice thicknesses of 0.6 m and winds of 10 m/s, the ice-ocean stress is ~0.3 N/m^2, and the magnitude contribution from the Coriolis influence is less than 8% of the total momentum budget. If we ignore this small contribution, the air-ice stress is balanced by the ice-ocean drag. Using a quadratic drag law for both stresses, the ice drift is then related to the wind velocity according to

$$|\mathbf{V}_i|e^{-i\beta} \approx c_{rt}|\mathbf{V}_a|e^{-i\delta} \qquad (3)$$

where $c_{rt} = (\rho_a c_a/\rho_w c_w)^{1/2}$ and $\beta = \delta$, so the ice speed is proportional to the wind speed, or $|\mathbf{V}_i| \approx c_{rt}|\mathbf{V}_a|$.

This exercise shows that a simple "rule-of-thumb" formula, in which the ice-water turning angle (β) is the average observed δ and the speed of the ice drift is simply a fixed fraction of the wind speed, may be quite applicable to the thin Antarctic pack ice. Such an approximation is often useful and is shown later to be surprisingly accurate.

3. DATA

The *Polarstern* entered the ice field on July 18, 1986, at approximately 59°S, 1°W and spent the following 2 months traversing the winter pack ice as shown in Figure 1. The

TABLE 1. Listing of Instrumentation Used in This Study With Model Numbers, Quantities Measured, Expected Accuracies, and Relevant Comments

Instrument	Model Number	Quantities	Accuracy	Remarks
Sonic-Anemometer-Thermometer (Kaijo Denki)	DAT-300	u', v', w', T'	0.005 m/s 0.025 °K	mounted on bow crane boom 15 m above ice
Doppler-SODAR system (Rosenhagen)	DS-100	wind velocity wind direction (vertical profiles)	0.5 m/s 5°	wind profiles ~30–250 m
INDAS data acquisition system (Theis)	THEIS 4.33 4.3303/3121	wind velocity wind direction	1 m/s 2.5°	measuring height 35 m
Doppler-SONAR system (Ametek)	DCP-4400/115	three-dimensional current profiles	~50 cm/s per point measurement	depth window ~30–150 m
Argos-Buoy system (Bergen Ocean Data)	UCM-10 Aanderaa 2740/2750	horizontal current wind velocity wind direction	2% full scale 2% 5°	10-m depth 2.1 m above ice (full scale 2.5 m/s)
Satellite navigation	Magnavox GPS	absolute position	±150 m (typical)	installed on *Polarstern*

types of data collected during this time relevant to this study are listed in Table 1. This table includes instrumentation, quantities measured, accuracy, and pertinent remarks.

Drift Stations

Three 4- to 5-day drift stations allowed collection of short time series during periods of ice-locked ship drift. These series, including the ship's drift track, provide the central data from which the drift and momentum parameters are derived. The ship's drift track serves as an accurate indicator of ice drift. This is demonstrated by comparing ship drift to the drift of an ice-locked meteorological Argos buoy deployed in the vicinity of the *Polarstern* during the initial hours of drift station 1. As seen in Figure 3, the buoy track compares well with that of the ship over the full 4.5 days and ~80 km of drift station 1.

Ice deformation studies conducted during the drift stations would have provided detailed information concerning local ice deformation but were hampered by equipment failures and noisy transponder signals. Consequently, internal ice stresses were not accurately measured, and information concerning periods of divergence and convergence is provided only by measuring the rate of change of the area encompassed by triangular buoy arrays (Figure 1). This gives an indication of the sense of deformation over broad areas in the study region. Because of the large scale however, this information only serves to aid in the interpretation of the local drift analyses. In general though, the centrally located buoy array, DFG (see Figure 1), present throughout most of the study, shows that the region is undergoing strong divergence interrupted by only two periods of significant convergence (Figure 4). Smaller scale convergence events are evident during the individual drift stations through closer examination of the areal change.

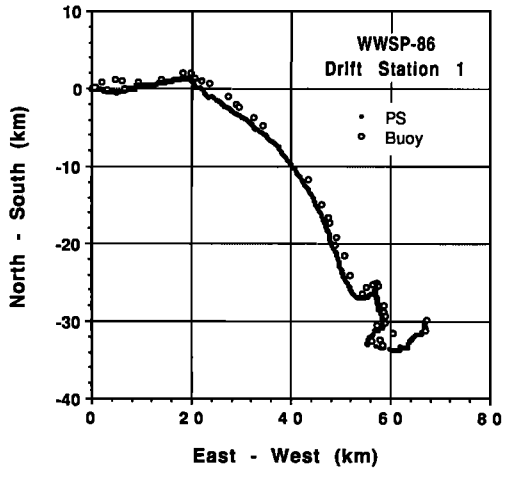

Fig. 3. Comparison between ship drift (PS) and a nearby (~2 km) ice-locked Argos buoy during drift station 1.

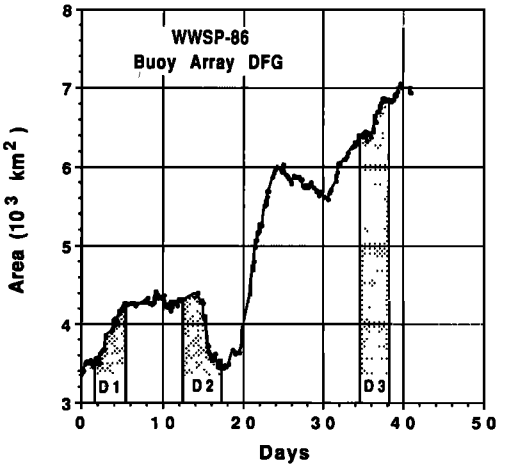

Fig. 4. Area contained within the triangle delimited by buoys D, F, and G (see Figure 1) as a function of time throughout most of the WWSP-86 expedition. Periods of large-scale divergence, in the vicinity of the buoy array, are suggested when the area increases with time, while a decrease suggests convergence. Most of the present analysis involves observations collected during drift stations 1, 2, and 3, which are indicated on the figure.

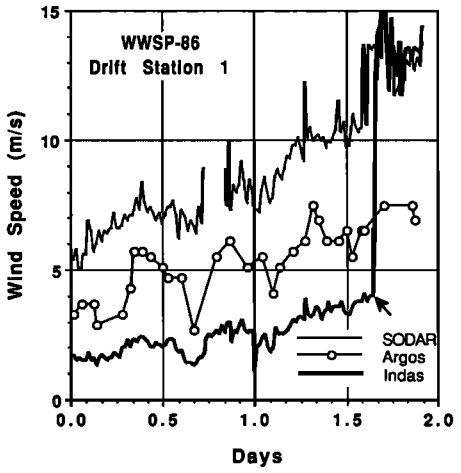

Fig. 5. Wind speeds measured during the first 2 days of drift station 1 by the shipboard INDAS system (bold curve) and Doppler SODAR system (light curve) at 35 m and by buoy-mounted cup anemometers at 2.1 m. Up until the time indicated by the arrow, the INDAS values are seen to be systematically lower than the SODAR values due to an icing problem. After correction of the problem, the offset was permanently removed. Note that the lower buoy wind speeds reflect their lower height; however, they too were observed to suffer from icing problems. The resulting systematic decrease in wind speed may serve to disguise corrupted values.

Wind Measurements

Wind velocity was continuously monitored by the ship's INDAS data acquisition system mounted on the mast approximately 35 m above the ice surface. These measurements were supplemented by those from a SONIC anemometer mounted at the end of a boom on the bow crane 15 m above the ice surface (this represents the lowest attainable reference height, which deviates slightly from the more standard 10-m height). To minimize ship effects, only those measurements taken when the winds approached from ±45° of the ship's heading were considered. Additional wind measurements were obtained from the bow mounted Doppler-SODAR system, which provided wind profile information over heights typically 30–250 m above the ice surface. These measurements were compared, when possible, with nearby Aanderaa cup anemometers and wind vane measurements mounted approximately 2.1 m above the ice surface on the ice-locked meteorological buoys.

The INDAS wind data were originally processed to provide 10-min averaged values. During the initial period of drift station 1, the INDAS anemometer suffered from an icing problem, which introduced a systematic reduction in wind speed as seen by comparison of the INDAS values to the 35-m height SODAR values (Figure 5). The icing was cleared and the problem solved half-way through the second day of the drift station, after which the INDAS and SODAR values agreed closely (Figure 5). The INDAS data corrupted by the icing were regressed on the SODAR values, providing a linear correction. The linearity of the icing problem is clear from the high correlation coefficient of 0.85 for this period.

Similar icing problems were observed to affect the cup anemometers mounted on the Argos buoys. These buoy wind speeds, consistently lower than the INDAS and SONIC values because of their lower level in the atmospheric PBL (ABL) were lowered further by collection, in the cups, of horizontally blowing snow. This influences their rotation rates in a systematic manner, possibly disguising corrupted wind speed values.

Following the correction for the icing period, the INDAS winds were adjusted to a 15-m height by regressing both speed and direction against the 15-m SONIC values. The regressions (Figure 6) show high linear correlations (0.981 for speed and 0.986 for direction), suggesting an excellent adjustment and avoiding any uncertainty in a theoretical adjustment. The height-adjusted (to 15 m) and icing-corrected winds for drift station 1, smoothed with a 1-hour wide filter (running average), are presented in Figure 7. Only the height corrections were required for each of the remaining two drift stations. Note that the analysis results are insensitive to the width of the wind filter.

Atmospheric Stress Measurements

Atmospheric stress was obtained throughout the field program by direct measurement of $u'w'$ (horizontal times vertical velocity fluctuations) using the SONIC measurements. Approximately 134 hours of stress measurements

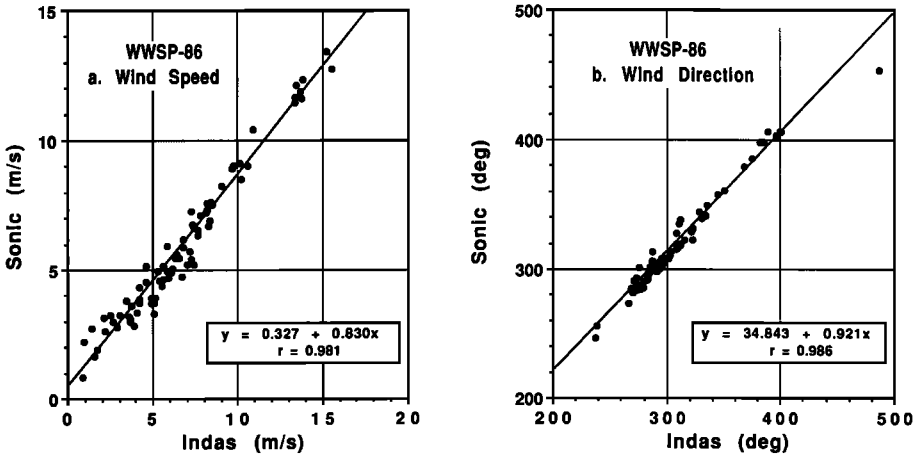

Fig. 6. Regressions relating INDAS 35-m height wind velocities to the 15-m SONIC values and used to adjust both the (*a*) speeds and (*b*) direction measurements to a 15-m reference level. The regression equations and correlation coefficients (*r*) are shown in the figures.

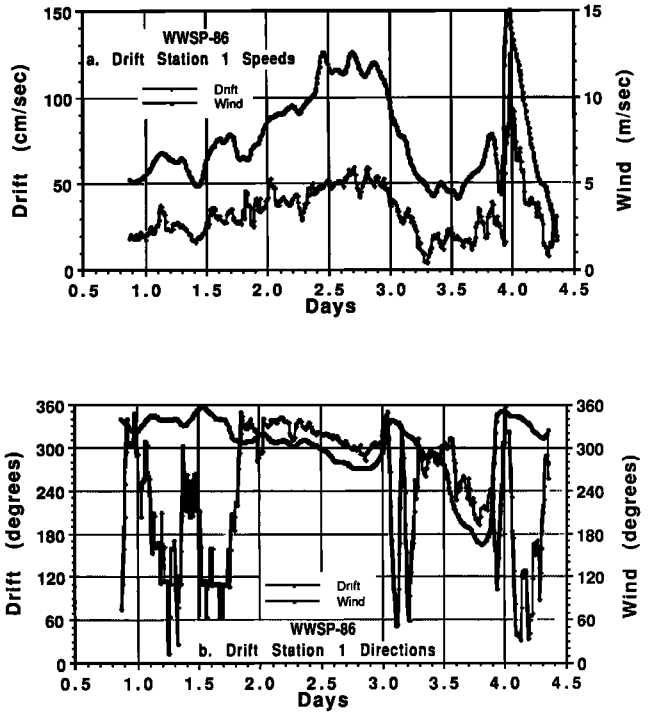

Fig. 7. The icing-corrected (during the first 2 days) and height-corrected wind speeds and directions for drift station 1. The observed ice drift speed and direction are included for comparison. The obvious correlation between the ice drift and winds anticipates the weak influence of the Coriolis force in the momentum balance, leading to a simple rule-of-thumb formula relating ice drift to wind velocity. Note that the rapid increase in speeds and directions just prior to day 4 reflects strong and rapid fluctuations in wind directions and satellite positioning errors which are amplified during storms.

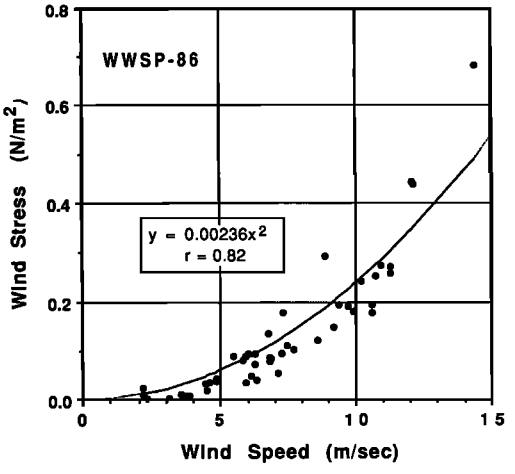

Fig. 8. Least squares quadratic fit to the wind stress versus wind speed data for 134 hours of direct stress measurements. This fit is constrained to pass through the origin. Note that the optimal power for these data is actually 2.2.

were made at the locations indicated along the cruise track in Figure 1. These measurements were divided into 268 half-hour intervals within which mean wind stress and 15-m wind speed were computed. The stress values were then regressed against the square of the wind speed (Figure 8) to determine the air-ice drag coefficient value for a standard quadratic drag law (though the optimal power was 2.2). The least squares fit, constrained to pass through the origin, yields a value of $c_a = (2.36 \pm 0.10) \times 10^{-3}$ ($\pm 1\sigma$; σ = 1 standard deviation) for the quadratic law and 15-m height winds. Since the standard errors computed for each half-hour interval were essentially the same, a weighted least squares regression was not required. Also, since >70% of these measurements were conducted during periods of neutral or unstable stratification due to the ventilation of heat from the ocean to the atmosphere, the influence of weak to moderate ground-based inversions [e.g., *Overland*, 1985] are considered to have a minimal influence on the drag coefficient value determined here.

Given the 15-m reference height and dependence of c_a on the inverse square of the wind speed suggests that the above value is smaller than a comparable 10-m height drag coefficient value; $c_{10} \approx 2.7 \times 10^{-3}$ using winds adjusted to a 10-m height with the formulation of *Guest and Davidson* [1987]. Though difficult to compare directly to Arctic values given the difference in conditions and wind speeds, 2.7×10^{-3} is typical of the small to medium floes (70–90% ice concentration) with vertical ridging and rafting reported by *Anderson* [1987]; it lies between *Guest and Davidson*'s [1987] c_{10} values for smooth to rough flows (70–90% ice concentration) and is consistent with *Overland*'s [1985] tabulated values derived from tower measurements over rough ice. This value is also consistent with *Andreas et al.* [1984], who predict in their Figure 10 that for 95% ice coverage in the Antarctic, c_{10} will be 2–2.5 times greater than the open ocean drag coefficient value, which they assume to be 1.2×10^{-3}, or $c_{10} \approx 2.4\text{–}3.0 \times 10^{-3}$.

Ocean Current Estimates

The momentum equation (1) is written in a Lagrangian framework in which the ice drift is described relative to the steady ocean flow below the level of OBL influence. In this open ocean region, the ocean approximates a homogeneous water column, and the circulation is likely dominated by barotropic flow with weaker baroclinic contributions. An estimate based on the Sverdrup circulation [*Gordon et al.*, 1981], representative of the barotropic flow, suggests average current speeds of ~1–2 cm/s. These values are consistent with estimates based upon winter mean dynamic topography [*Gordon et al.*, 1978].

Direct measurements of the current by a current meter chain, designed for deployment through the ice during the drift stations, was unsuccessful, as the chain was lost during the trial deployment following the passage of an intense storm. This left the Ametek Doppler Sonar shipboard profiler. This system was subject to a very poor signal-to-noise ratio (~5 times worse than the expected 50-cm/s point measurement error) and was incapable of providing valid velocity profile information. However, its high-density sampling in both space and time allows a stable statistical estimate of the mean flow over a broader depth and time interval. The system has sampling intervals of 2.5 s and 6.4 m over a depth window of ~30–150 m. Initial processing over half-hour intervals (720 samples) showed a large scatter with an estimated error of approximately ±10 cm/s. Mean velocity estimates were recomputed for nonoverlapping 40-min windows over a 30- to 100-m depth range (~10,500 samples). Given that the magnitude of the error decreases

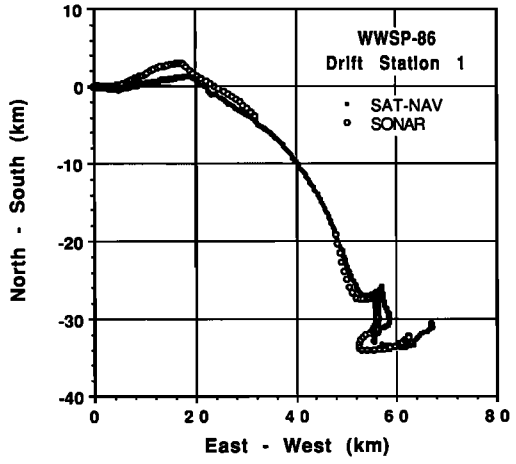

Fig. 9. Observed drift track versus that predicted using ocean Doppler SONAR predicted drift velocities (averaged over 30- to 100-m depth and 40-min time intervals). These velocities are relative to the steady ocean current below the PBL, so differences between the observed and predicted drift tracks are an indication of the magnitude of error (2.3 km rms) expected by ignoring the ocean currents in the drift analyses. Note that the inconsistent sense of the mismatch is not expected from a steady ocean current.

with $n^{-1/2}$, this increased sample size reduces the error by a factor of 3.8 to a value of ±2.6 cm/s for the broader depth window. The averaging however, does not overcome systematic errors associated with miscalibration problems.

These mean sonar velocities represent ice drift speed relative to the mean ocean current flow below the depth of significant OBL influence. Over 18 hours of near-steady conditions, they show a linear correlation to the satellite navigation (i.e., absolute) ship drift velocities of 0.98 with a linear slope of 0.97 ± 0.03 and an offset of 0.7 ± 2.6 cm/s. The offset represents the average ocean current speed and is consistent with the above estimates. However, its large uncertainty (highly indistinguishable from zero) and the small magnitude of such predicted current speeds relative to typical ice drift velocities (<5%) lead us to ignore its influence when analyzing the ice drift.

Neglecting the ocean current may thus introduce an error of the magnitude visually indicated in Figure 9. This shows the drift track for drift station 1 predicted using the Ametek Sonar average velocities versus the observed (absolute) drift track. The difference between the two tracks is presumably due to the ocean current, which is not included in the drift track produced using the sonar velocities. The average magnitude of the mismatch between the two tracks, given by the rms error, is 2.3 km. Since one would expect the mean current to introduce a systematic offset between the two tracks, the changing nature of the mismatch suggests factors other than a steady ocean current.

Finally, in addition to the above, current meters suspended at 10-m depth from two ice-locked meteorological Argos buoys in the vicinity of the ship provide nominal information concerning the velocity shear in the OBL. These allow a qualitative check of the true drag coefficient estimates.

4. Analysis

Quadratic Drag Law Parameters

The optimal values of the quadratic drag law parameters, c_w and β, and associated errors are sensitive to the actual methodology employed to extract the values from the data. Consequently, we consider two methods of estimating the values. Ideally, c_w and β are extracted by inversion of the quadratic form of the free drift equation:

$$if|\mathbf{V}_i| + \alpha|\mathbf{V}_i|^2 e^{-i\beta} = \gamma|\mathbf{V}_a|^2 e^{-i\delta} \tag{4}$$

where $\alpha = \rho_w c_w/m_i$ and $\gamma = \rho_a c_a/m_i$.

This equation is nonlinear with respect to β, but it can be decomposed and rearranged to provide two linear regression equations of the form $y_i = a_i x_i$ ($i = 1, 2$ corresponding to (5*a*) and (5*b*), respectively):

$$|\mathbf{V}_i| = \left(\frac{\rho_a c_a}{\rho_w c_w}\right)^{1/2}\left(\frac{\cos\delta}{\cos\beta}\right)^{1/2}|\mathbf{V}_a| \tag{5a}$$

$$\frac{(\cos\delta\cos\beta)^{1/2}}{\sin(\delta-\beta)} = \frac{(\rho_a c_a \rho_w c_w)^{1/2}}{m_i f}|\mathbf{V}_a| \tag{5b}$$

with $a_1(c_w) = (\rho_a c_a/\rho_w c_w)^{1/2}$ and $a_2(c_w) = (\rho_a c_a \rho_w \cdot c_w)^{1/2}/m_i f$. Note that these equations can be rearranged to yield several different configurations of the regression variables y_i and x_i. The forms shown here provide the clearest separation of the external parameters and serve to align the variables so as to minimize the rms scatter of the fit. These forms also force the regression line to pass through the origin, though (5*b*) is singular there. This is consistent with (4) and indicates that $|\mathbf{V}_i|$ is zero when there is no wind (recall that $|\mathbf{V}_i|$ is relative to the geostrophic current) and that the turning angles have no meaning when there is no wind or ice drift (i.e., there is no meaningful intercept at all, zero or otherwise).

Simple solutions exist for the coefficients a_1 and a_2 for specified β, so each equation is solved to yield a function $c_w(\beta)$ by generating solutions for a range of β. The intersection of these two $c_w(\beta)$ yields an optimal fit of c_w and β to the observed wind and ice drift data. For (5*a*) the regression must be constrained to pass through the origin.

Though this approach is computationally attractive, considerable care is required in setting up and computing the regressions and associated errors. General evaluation of the regressions and resulting $c_w(\beta)$ functional forms suggests the following considerations. First, the function $c_w(\beta)$ resulting from (5*a*) is well behaved and shows little variation in c_w over a wide range of β. Examination of the associated regression variables, however, reveals a poor correlation due to noise in the data which is amplified and skewed by the nonlinear nature of x_1. Consequently, the regression coefficient a_1 is subject to distortion and a large error which, when propagated to c_w, undermines the otherwise robust solution regardless of the precision with which β is known. Typical magnitude of this error is $O(10^{-3})$.

For (5*b*) the regression variables are better correlated, but the highly nonlinear form of y_2, dominated by $\sin(\delta-\beta)^{-1}$, causes this term to grow disproportionately large where $\delta - \beta$ approaches zero. These points serve as strong leverage points which significantly influence (pull) the regression line from the stable fit. This leads to oscillatory behavior and discontinuities in $c_w(\beta)$ which severely degrade the convergence. The problem is effectively overcome by employing a robust correlation technique such as the least median of squares method [*Rousseeuw and Leroy*, 1987], which ignores the leverage points. This allows a smooth conver-

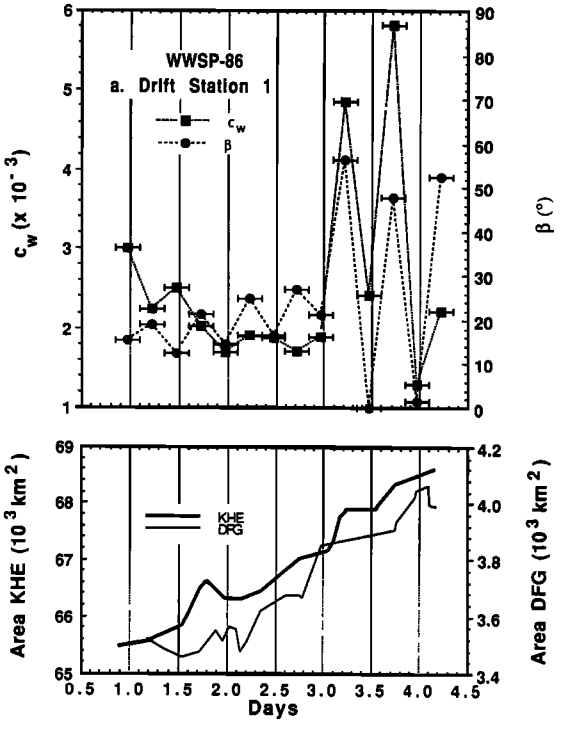

Fig. 10*a*

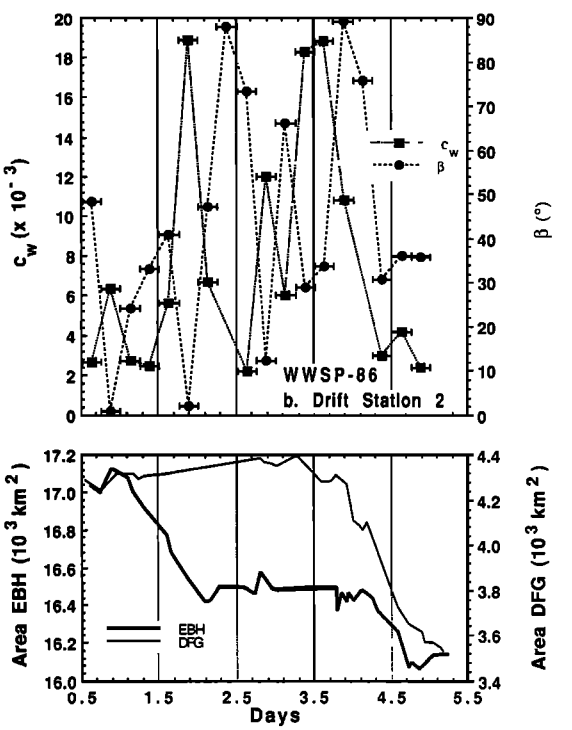

Fig. 10*b*

Fig. 10. Numerically optimized values (L1 norm) of the quadratic drag coefficient and turning angle for 6-hour, nonoverlapping segments (indicated by horizontal bars) along the drift track for (*a*) drift station 1, (*b*) drift station 2, and (*c*) drift station 3. Sense of the large-scale divergence at the time of the measurements is also indicated (as described in Figure 4) in the lower panel. Locations of buoy arrays used to estimate the degree of divergence are shown in Figure 1.

gence, but the precision with which c_w and β are resolved is still low (this is true for c_w even if β is known exactly) because the large scatter in the external scalar fields defining the regression variables leads to skewed correlations and poorly defined regression minima. Also, the intersection between the $c_w(\beta)$ functions is fairly shallow and over a broad zone which strongly contributes to a low precision in defining the value of β. Therefore this method appears to be best suited for small sections of data over which conditions are fairly stable and the noise relatively low.

An alternative approach to determining c_w and β is through a numerical minimization of the error between the observed and predicted drift tracks as a function of specified parameter values. Conceptually, by directly minimizing the predicted drift vector error, this approach, though it suffers from its computationally tedious nature, offers the advantage of reducing the sensitivity to random scalar noise which plagues the above method.

The numerical approach involves minimization of the L1 norm, though solutions were also obtained by minimizing the L2 norm and a modified L1 "norm" in which the actual difference, as opposed to magnitude, was summed. The different norms were used in an attempt to find the optimization most suited for the vector data and to assess the sensitivity of the results to the form used to describe the mismatch (see *Menke* [1984] for a review of norms). It was found that the differences between the various results are insignificant except in extremely noisy cases in which the L1 norm is somewhat more robust, as expected.

For comparison of techniques, the best numerical optimization estimates for drift station 1 were compared with those obtained using the regression equations (*5a*) and (*5b*). The optimum numerical values for this station are $c_w = (1.83 \pm 0.6) \times 10^{-3}$, $\beta = 18.9° \pm 17°$, and the regression results are $c_w = (1.53 \pm 0.6) \times 10^{-3}$, $\beta = 25° \pm 12°$. So while the errors for both estimates are similar, the regression-derived values show a distinctly lower drag coefficient and higher ß. The ice drift vectors computed using these two different estimates show rms errors relative to the observed drift track of 1.5 and 6.9 km for the numerically and regression-derived values, respectively. The better fit by the numerically derived values is not surprising, since they represent those values which minimize this error. However, because the rms error is a direct measure of the success of the free drift equation in describing the observed ice drift vector, the numerically derived values are considered to be better.

In order to differentiate between estimates of true c_w and β from those representing effective values (during periods of significant ice interaction), optimum values were computed over short segments of each drift track. This allows an examination of c_w and β as they vary with time along the track, which is useful in detecting the influence of ice interaction. Those estimates considered representative of periods of true free drift are then combined to produce the best values and confidence intervals for true c_w and β.

The optimal segment width was determined by experimenting with a variety of overlapping widths ranging from 4 to 12 hours. These experiments show that for segments less than 6 hours, the number of data points used in the optimization is too small to consistently yield stable estimates (the modified L1 norm was unstable over a couple of particularly noisy segments even for the 6-hour segment length). Wider

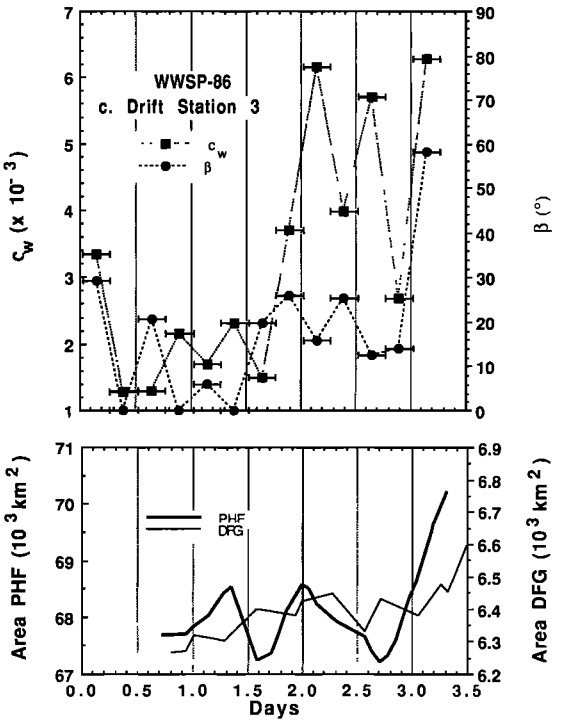

Fig. 10*c*

segments essentially produced smoothed versions of the 6-hour segment estimates. Therefore the 6-hour segments represent the minimum width allowing fairly stable parameter estimates and thus the optimal segment width.

The data for each of the three drift stations were broken into 6-hour nonoverlapping segments, and the optimum values of c_w and β were computed for each. These results were compared (Figure 10) with the ice convergence information for the same periods of time in an effort to differentiate between periods of divergence and convergence. As seen in Figure 10*b*, drift station 2 appears to represent a period of large-scale ice convergence. Local convergence over a 46-hour period at this time was also suggested by a ~10% decrease in local ice area as observed during a brief period when the near-ship transponders were functioning. This convergence coincides with a period in which the entire northern ice limit was shifted approximately 5° to the south as revealed by microwave satellite data (J. Comiso, personal communication, 1988).

True drag values. Estimates of the true drag law parameter values (representing steady OBL conditions) require isolation of those track segments most representative of free drift conditions. Examination of the results for drift stations 1 and 3 (Figures 10*a* and 10*c*) shows no consistent relationship between high drag coefficients and periods of large-scale convergence over the 6-hour segments. High values for some periods of large-scale divergence probably reflect local ice interaction, while low values during periods of large-scale convergence may simply reflect nonconverging local conditions. Because the buoy arrays only indicate large-scale convergence/divergence, it is difficult to clearly identify periods of true free drift. Therefore we arbitrarily chose periods of free drift as those during large-scale divergence which coincide with values of $c_w < 2 \times 10^{-3}$.

The 10 estimates satisfying these criteria show a nearly Gaussian distribution (the means and median values are similar, as are estimates of the error), so the mean value is chosen to allow a reasonable estimate of the scatter. These values are $c_w = (1.62 \pm 0.24) \times 10^{-3}$ and $\beta = 15.2° \pm 9°$. Alternatively, one might argue that the best estimate of the true drag values are given by the lowest measured values. The lowest stable ($\beta > 2°$) value is $c_w = 1.3 \times 10^{-3}$ with $\beta = 20.7$. Given that this value lies beyond the confidence interval estimated above, we suggest working with the mean value with serious consideration of the potential error. Also, averaging the 10 estimates, representing 60 hours of drift, reduces the noise introduced during individual 6-hour segments of true free drift in which OBL transient behavior is not suppressed by ice interaction. This transient behavior may account for the large scatter in β.

The WWSP-86 data are inadequate to resolve the OBL structure and allow a reasonable theoretical estimate of c_w and β. However, the characteristics of the OBL can be estimated by making simple assumptions regarding its nature and by using the estimates of true c_w, β, and measured OBL velocities. The velocity data were collected during 18 hours of near-steady conditions by current meters suspended at ~10-m depth from two ice-locked buoys. Since the current meters were being dragged through the OBL at speeds averaging~30 cm/s, the measured velocities represent vector differences of the ice drift and actual OBL 10-m velocity component. Correlations of the current meter and ice drift velocity components indicate that the 10-m current speed is ~38% of the surface drift speed for both data sets. The relative angle, however, between the ice and 10-m current direction cannot be reliably determined. One data set shows a +17° angle from the ice drift, and the other a −19° angle. This is likely due to a small signal-to-noise ratio reflecting the strength of the ice drift component in the current meter signal.

Consistent with a quadratic drag law, we assume a two-layer OBL in which the inertial sublayer, characterized by a linearly increasing eddy diffusivity, overlies the outer Ekman layer. *McPhee* [1979] finds that a Rossby similarity scaling of the steady OBL momentum equation is most appropriate for his Arctic observations. The true advantage of this scaling is lost in the present analysis, since our data represent near-steady conditions with a single friction velocity (u_*). The scaling owes its advantage to its treatment of the depth of the inertial sublayer z_N, which is scaled to vary with u_*. However, while u_* does not vary in the present case, the concept of the universal maximum nondimensional mixing length, $\xi_N = c_w/(2k \sin^2 \beta)$ (k is von Karman's constant) central to the scaling is still useful to determine the depth of the inertial sublayer z_N.

Using the Rossby similarity scaling, with $c_w = 1.62 \times 10^{-3}$, $\beta = 15.2°$, and $u_* = 0.01$ m/s, then $\xi_N \approx 0.03$, or $z_N \approx 2.2$ m, and the surface roughness length, $z_0 \approx 2$ mm. Consideration of the potential errors in the values of c_w, β, and u_* suggest that $1 \lesssim z_N \lesssim 15$ m and $z_0 < 4$ mm.

Effective drag values. Estimating single, most representative values of effective c_w and β which subsume the influence of "typical" Antarctic ice interaction is difficult due to the nonlinear nature of **I** in (1). This is evidenced by comparing the median and mean of the individual segment estimates for each drift track to the optimal values (presented in Table 2) computed by fitting each track in its entirety. These comparisons show that the median values are 4–22%

TABLE 2. Summary of Estimated Parameter Values for the Various Formulations Considered

Estimate	Formulation		
	Quadratic (Equation (4))	Linear (Equations (7) and (10))	Rule-of-Thumb (Equation (3))
Best true values	$c_w = (1.62 \pm 0.24) \times 10^{-3}$*	$c_w^1 = (0.80 \pm 0.06) \times 10^{-3}$	
		$(c_a^1 = 26.55 \times 10^{-3})$	
	$\beta = 15.2° \pm 9.0°$*	$\beta = 18.1°$	
Best overall effective values	$c_w = (3.22 \pm 1.48) \times 10^{-3}$*	$c_w^1 = (1.48 \pm 0.35) \times 10^{-3}$	$c_{rt} = 0.0303 \pm 0.008$
		$(c_a^1 = 35.4 \times 10^{-3})$	
	$\beta = 18.1° \pm 1.7°$*	$\beta = 19.6° \pm 1.3°$	$\beta = 23.4° \pm 1.3°$
Drift station 1	$c_w = 1.83 \times 10^{-3}$	$c_w^1 = 0.83 \times 10^{-3}$	$c_{rt} = 0.0401$
	$(c_{wp(6a)} = 1.75 \times 10^{-3})$	$(c_{wp(10)}^1 = 0.85 \times 10^{-3})$	$(c_{rtp(3)} = 0.0401)$
	$(c_{wp(6b)} = 1.60 \times 10^{-3})$	$(c_{wp(7)}^1 = 0.83 \times 10^{-3})$	
		$(c_a^1 = 26.55 \times 10^{-3})$	
	$\beta = 18.9°$	$\beta = 20.7°$	$\beta = 25.2°$
	$\text{rms}_b = 1.5$	$\text{rms}_b = 1.4$	$\text{rms}_b = 1.4$
	$\text{rms}_s = 11.9$	$\text{rms}_s = 11.6$	$\text{rms}_s = 11.8$
Drift station 2	$c_w = 5.26 \times 10^{-3}$	$c_w^1 = 1.89 \times 10^{-3}$	$c_{rt} = 0.0241$
	$(c_{wp(6a)} = 5.23 \times 10^{-3})$	$c_{wp(10)}^1 = 1.89 \times 10^{-3})$	$(c_{rtp(3)} = 0.0237)$
	$(c_{wp(6b)} = 5.13 \times 10^{-3})$	$(c_{wp(7)}^1 = 1.96 \times 10^{-3})$	
		$(c_a^1 = 35.4 \times 10^{-3})$	
	$\beta = 19.7°$	$\beta = 19.8°$	$\beta = 21.8°$
	$\text{rms}_b = 4.1$	$\text{rms}_b = 4.0$	$\text{rms}_b = 3.9$
	$\text{rms}_s = 8.4$	$\text{rms}_s = 8.7$	$\text{rms}_s = 8.4$
Drift station 3	$c_w = 2.56 \times 10^{-3}$	$c_w^1 = 0.99 \times 10^{-3}$	$c_{rt} = 0.0339$
	$(c_{wp(6a)} = 2.63 \times 10^{-3})$	$(c_{wp(10)}^1 = 1.00 \times 10^{-3})$	$(c_{rtp(3)} = 0.0339)$
	$(c_{wp(6b)} = 2.88 \times 10^{-3})$	$(c_{wp(7)}^1 = 0.98 \times 10^{-3})$	
		$(c_a^1 = 26.55 \times 10^{-3})$	
	$\beta = 15.8°$	$\beta = 18.2°$	$\beta = 22.0°$
	$\text{rms}_b = 2.9$	$\text{rms}_b = 2.5$	$\text{rms}_b = 2.5$
	$\text{rms}_s = 4.7$	$\text{rms}_s = 4.0$	$\text{rms}_s = 4.2$

Values presented for individual drift stations include optimal values (computed by numerical minimization) and predicted values. Predicted values are indicated by subscript pn, where n is the number of the equation used to make the prediction. Also given is the rms error between observations and simulations using the optimum parameter values (rms_b) and the corresponding best overall effective value (rms_s). Figures 11–13 show the predicted drift tracks from which these rms errors arise. Linear drag coefficients (c_w^1) have units of m/s and are a function of the air-ice drag coefficient values (c_a^1), estimated from (7*b*).

*Best values.

larger than the optimal values and the mean values are 21–39% larger. While the more robust median value estimates are closer to the optimal values, they still overestimate the effective values determined when considering the drift tracks in full. Therefore we simply average the optimal values of each of the three drift tracks to provide an estimate of representative values of effective c_w and β. This averaging yields $c_w = (3.22 \pm 1.48) \times 10^{-3}$ and $\beta = 18.1° \pm 1.7°$. These values are within 18% of the median value estimates determined using all 6-hour segment estimates.

The consequence of employing a single effective value to describe typical Antarctic pack ice drift is indicated by comparing the rms error between predicted and observed drift tracks using the optimal parameter values for each individual drift station and the overall effective values. The results of this comparison are summarized in Table 2 and Figures 11–13. As shown by these results, the rms error increases by as much as a factor of 8 for drift station 1 and by a factor of $\lesssim 2$ for both drift stations 2 and 3.

Given that the effective values include the influence of ice interaction, one might expect a correlation between these values and the degree of ice divergence. As discussed above, there is no obvious relationship between c_w and the large-scale divergence over the 6-hour window estimates. However, comparison of the optimal effective c_w for the full 4–5 days of each drift station to the average degree of divergence over that same full period shows a very strong correlation, though one that is dependent on the scale over which the divergence is measured.

Table 3 shows the optimum effective c_w for each drift station and the average divergence over the same period as measured over a relatively small area (buoy array DFG; ~ 3–7×10^4 km^2) and over a larger area (buoy arrays KHE, EBH, or PHF; ~ 16–70×10^4 km^2, consistent with the lower panels of Figure 10). The scale dependence reveals gradients in the divergence field. In both cases though, the correlation between c_w and the divergence is very good. For the smaller scale divergence the magnitude of correlation is 0.985, and for the larger scale it is 0.998 with the regressions given by

$$c_w = a_j(\nabla \cdot \mathbf{V}_i)_j + b_j \tag{6}$$

where $j = a, b$ represents the small- and large-scale coefficients, respectively, and $a_a = -2845.91$, $b_a = 3.365 \times 10^{-3}$; $a_b = -10{,}247.34$, $b_b = 3.490 \times 10^{-3}$.

The values of effective c_w predicted by (6) are included in Table 2. For the small-scale divergence, the predicted values are within $\sim 12\%$ of the optimal values, and for the large-scale divergence they are within 5%. Treating the effective c_w as a simple linear function of large-scale (easily measured) divergence offers some considerable modeling advan-

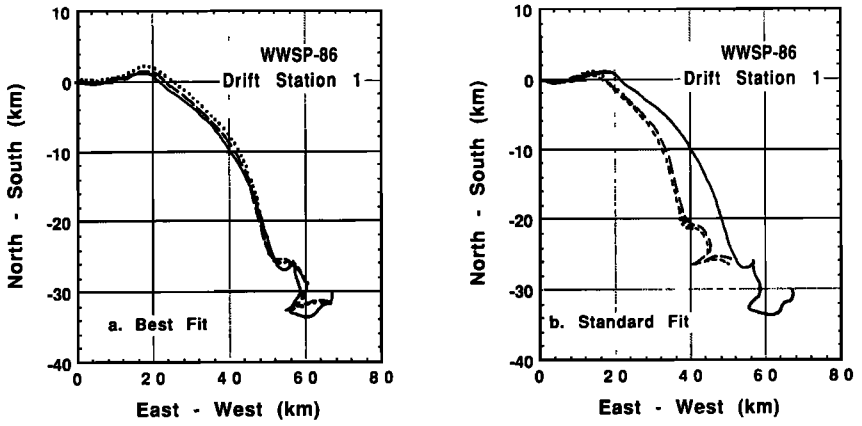

Fig. 11. Predicted versus observed drift tracks for drift station 1. Predictions use free drift equation with quadratic drag law (dotted line), linear drag law (dashed line), and simple rule-of-thumb formula (long-dashed line) in which ice drift is proportional to wind speed. The solid line represents the observed ice drift. (*a*) Model parameters are computed by numerical optimization to produce the best fit to observed drift. Notice that all three model formulations are essentially indistinguishable (all have rms errors within a few percent of one another; see Table 2 for rms values). (*b*) Model parameters are average of those for all three drift stations (overall best effective values in Table 2). These are therefore the "representative" values for typical Antarctic conditions. Note, where the predicted rule-of-thumb, quadratic, and linear predicted drift tracks overlap, only the long dashes are shown. Similarly, where the linear drift track overlaps another track, only the other track symbol is shown. For time reference, the corresponding bends and curves of the predicted and observed tracks are essentially synchronous.

tages. However, these regressions are based upon only three 4- to 5-day drift stations, and while they represent a large spread in the degree of divergence/convergence, further observations are obviously required to refine the coefficients, the errors and limitations, as well as the nature/consistency of the scale dependence.

Linear Drag Law Parameters

Estimates of the linear parameter values can be obtained with the same methods employed to determine the quadratic values. Alternatively, if one considers the linear power law an approximation to the quadratic law over a limited range of forcing and can tolerate a specified β, the linear drag coefficient can be determined directly from the quadratic values. This is an appealing prospect, since the quadratic values are most frequently presented in the literature.

The linear value is extracted from the quadratic value by simply performing a (continuous) least squares linear fit to the quadratic curve. That is, minimize the error integral

$$E = \int_{U_l}^{U_u} [\tau_l(U) - \tau_q(U^2)]^2 \, dU$$

where $\tau_l(U) = c_D^l U$ (the linear fit), $\tau_q(U^2) = c_D U^2$ (the quadratic fit), c_D^l represents the air-ice (c_a^l) or ice-water (c_w^l) linear drag coefficient value, c_D is the quadratic value (c_a or c_w), U_u is maximum ice drift (for c_w^l) or wind speed (for c_a^l), and U_l is minimum speed. Because the least squares fit minimizes the rms error over the entire range of the fit, the linear fit to a quadratic curve is most valid if the range of speeds encompasses those from which the quadratic curve was determined.

The least squares solution is given by

$$c_D^l = c_D \left[\frac{3(U_u^4 - U_l^4)}{4(U_u^3 - U_l^3)} \right] \tag{7a}$$

or, if $U_l \approx 0$,

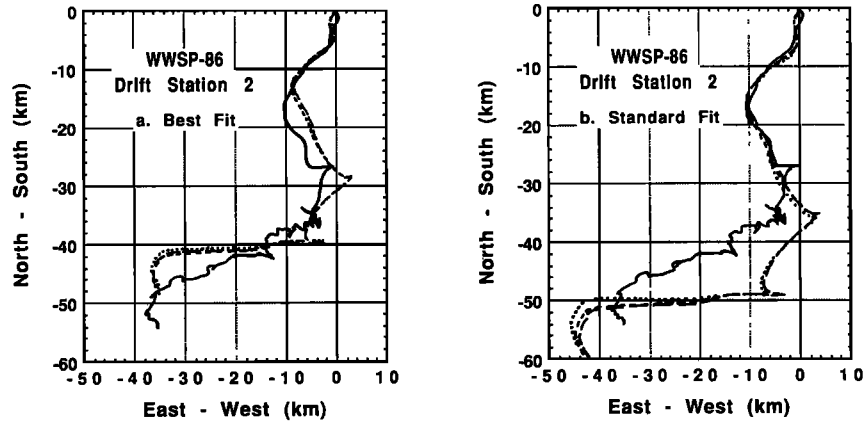

Fig. 12. As for Figure 11 using drift station 2 data.

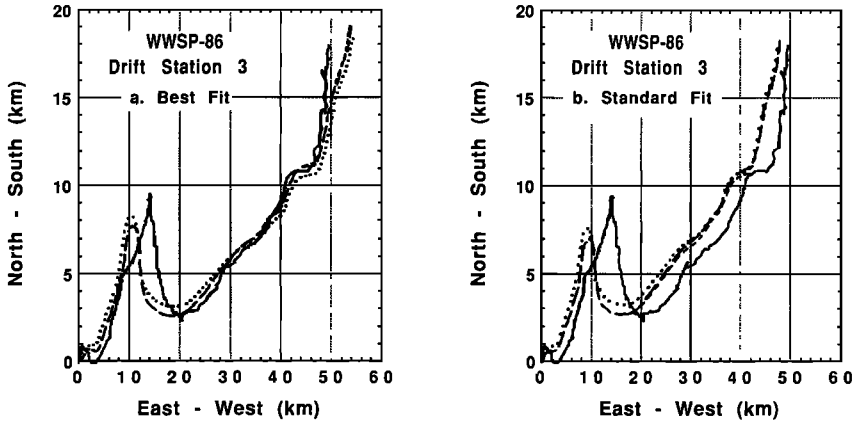

Fig. 13. As for Figure 11 using drift station 3 data.

$$c_D^1 = c_D \frac{3U_u^4}{4U_u^3} \tag{7b}$$

As presented, the linear fit is constrained to pass through the origin and is fairly sensitive to the maximum wind or drift speed U_u. Relaxing the constraint of passing through the origin requires that $\tau_1(U) = c_D^1 U + \tau_{U_1}$ in the error integral, where τ_{U_1} is the intercept stress at the lower wind speed limit U_1. In this case the least squares solution is given by

$$c_D^1 = c_D \left[\frac{3(U_u^4 - U_1^4)\Delta U - 2(U_u^2 - U_1^2)(U_u^3 - U_1^3)}{4(U_u^3 - U_1^3)\Delta U - 3(U_u^2 - U_1^2)^2} \right] \tag{7c}$$

$$\tau_{U_1} = \frac{2c_D(U_u^3 - U_1^3) - 3c_D^1(U_u^2 - U_1^2)}{6\Delta U} \tag{7d}$$

This form gives a better absolute approximation to the quadratic values. However, as is shown below, the absolute value of c_D^1 is not as important as is the ratio of c_a^1/c_w^1. Therefore equations (7*a*) and (7*b*) suffice, and use of (7*b*) is usually justified even for ranges in which the minimum speed is significantly larger than 0.

Proper use of the linear approximation requires that both the air-ice and ice-water drag laws be approximated as linear. This is shown by equating the linear solution (for magnitude) of the free drift equation to the quadratic solution. Since the linear drag values represent an approximation to the quadratic drag law, these two solutions must be equal. Using a quadratic air-ice drag law in combination with the linear ice-water drag then gives

$$\frac{\gamma |\mathbf{V}_a|^2}{f(\alpha_1^2 - 2\alpha_1 \sin\beta + 1)^{1/2}} = \left(\frac{\gamma}{\alpha}\right)^{1/2} \left(\frac{\cos\delta}{\cos\beta}\right)^{1/2} |\mathbf{V}_a| \tag{8}$$

where $\gamma = \rho_a c_a / m_i$, $\alpha_1 = \rho_w c_w^1 / m_i f$, and $\alpha = \rho_w c_w / m_i$. Solving this equation for c_w^1 (ignoring $(\cos\delta/\cos\beta)^{1/2}$, which is good to ~2%) gives

$$c_w^1 = \frac{-m_i f \sin\beta}{\rho_w} + \left(\frac{\rho_a c_a c_w}{\rho_w} |\mathbf{V}_a|^2 - \frac{m_i^2 f^2 \cos^2\beta}{\rho_w^2} \right)^{1/2}$$

or, since $\rho_a c_a c_w / \rho_w |\mathbf{V}_a|^2 \gg m_i^2 f^2 \cos^2\beta / \rho_w^2$ (by ~2 orders of magnitude),

$$c_w^1 \approx \frac{-m_i f \sin\beta}{\rho_w} + \left(\frac{\rho_a c_a c_w}{\rho_w} \right)^{1/2} |\mathbf{V}_a| \tag{9}$$

This shows the linear drag coefficient c_w^1 to be nonconstant with a functional dependence on $|\mathbf{V}_a|$. Alternatively, rewriting (8) using a linear drag for the air-ice stress on the left-hand side and solving for c_w^1 gives

$$c_w^1 \approx \frac{-m_i f \sin\beta}{\rho_w} + c_a^1 \left(\frac{\rho_a c_w}{\rho_w c_a} \right)^{1/2} \tag{10}$$

where the same constant term as in (9) has been neglected. Equation (10) now shows a constant c_w^1, which for a specified value of β, can be used in place of (7) to estimate the optimal linear ice-water drag coefficient value (note that c_a^1, however, must still be estimated from (7)). For thin ice such as that encountered in the Antarctic, the first term on the right-hand side of (10) contributes only 1–3% to the value of c_w^1. It can therefore be ignored (for 3-m-thick ice its contribution can reach ~20%), so $c_w^1 \approx c_a^1 (\rho_a c_w / \rho_w c_a)^{1/2}$. This shows that the ratio of c_w^1/c_a^1 is constant and c_w^1 is adjusted according to the value of c_a^1. Consequently, for the linear case, this explicitly supports the suggestion by *McPhee* [1980] and findings of *Pease et al.* [1983] that the ratio of the drag coefficients is more important than the absolute values.

Equations (7) and (10) are tested by comparing their predicted values of c_w^1 for drift station 1 to the numerically determined optimum value. The optimum value is $c_w^1 = 0.83 \times 10^{-3}$ m/s ($\beta = 20.7°$). Equation (7*b*) using a quadratic c_a =

TABLE 3. Optimum Quadratic Drag Coefficient Values for Each Drift Station and Average Divergence During the Drift Station Period

Drift Station	Optimum c_w	Divergence "Small" Scale	Divergence "Large" Scale
1	1.83×10^{-3}	6.2×10^{-7}	1.7×10^{-7} (KHE)
2	5.26×10^{-3}	-6.2×10^{-7}	-1.7×10^{-7} (EBH)
3	2.56×10^{-3}	1.7×10^{-7}	0.84×10^{-7} (PHF)

Small-scale divergence values have been determined from the change in area encompassed by buoy array DFG (see Figure 1), and large-scale divergences are from the buoy arrays indicated in parentheses. Divergences have units of s^{-1}.

2.36×10^{-3} and maximum wind speed (U_u) 15 m/s, yields $c_a^1 = 26.55 \times 10^{-3}$ m/s. Using this value of c_a^1 in (10) gives $c_w^1 = 0.85 \times 10^{-3}$ m/s, while (7*b*) gives $c_w^1 = 0.83 \times 10^{-3}$ m/s (maximum ice drift speed ~60 cm/s). The results of this test as well as that for the other two drift stations are summarized in Table 2. The predicted c_w^1 values from both (7) and (10) are seen to be consistently good (within ≤2% of the optimal value). The results thus indicate that the linear drag coefficient can be directly determined from the quadratic drag coefficient using either (7) or (10) (though (10) is preferable for stability reasons).

Given the success of (7) and (10) for the individual drift stations, we estimate the best overall effective linear drag law coefficient by combining all wind speed data to determine c_a^1 from (7) (maximum wind speed ≈20 m/s), giving $c_a^1 = 35.4 \times 10^{-3}$ m/s. Equation (10) then yields the best overall effective $c_w^1 = (1.48 \pm 0.35) \times 10^{-3}$ m/s. The error is computed by inserting the upper and lower quadratic drag coefficient confidence limits into (10) and averaging for symmetry (introducing an ~18% error into σ). The best corresponding β is simply the average for the three drift stations, 19.6° ± 1.3° (the error simply reflecting the observed scatter in the optimal fits of the three drift stations). For the true linear drag coefficient value, $c_w^1 = (0.80 \pm 0.06) \times 10^{-3}$ m/s and $\beta = 18.1°$ (no error computed). These values are summarized in Table 2.

Comparison of the rms error between predicted and observed drift using the optimal linear parameter values for each drift station versus the overall effective values are given in Table 2 and Figures 11–13. These results show that use of the overall effective values increases the rms error by a magnitude similar to that in the quadratic case above. More important, the results show that the rms error for the linear drag law parameter values are essentially indistinguishable from those for the quadratic values. Thus the linear drag laws represent an excellent approximation to the quadratic drag law over a broad range in the forcing.

Ice-ocean momentum exchange. The effective drag coefficient values are only good for use in modeling the ice drift and estimating the degree of momentum exchange from the atmosphere to the ice. These values cannot be used as a forcing in ocean modeling, since their inflated size represents the additional momentum loss due to ice interaction, not to an enhanced ice-water drag, as implied by the free drift formulation. To properly consider the momentum transfer to the ocean, the ice velocity must be computed using the effective (enhanced) drag coefficient values, after which this velocity is used with the true drag coefficient to estimate the ice-water stress driving an ocean circulation (note that the ice-water stress driving the ocean takes the opposite sign relative to the ice-water stress acting as a drag on the ice).

In other words, we must remove the ice interaction from the ice-water stress. *Hibler and Bryan* [1984] did this explicitly in their coupled ice-ocean model. Here, since the ice interaction is included in the effective drag, we must remove it in a stepwise fashion as described above or directly in the following manner. First, the solution of the linear drag law formulation of the free drift equation gives the relationship of $\mathbf{V}_i$, determined using the effective drag coefficients, to the air-ice stress:

$$\mathbf{V}_i = \frac{\boldsymbol{\tau}_a^1}{f(\alpha^2 - 2\alpha \sin \beta + 1)^{1/2}} e^{-i\delta} \tag{11}$$

where $\boldsymbol{\tau}_a^1$ is the air-ice stress computed using a linear drag law and $\alpha = \rho_w c_{we}^1 / m_i f$, c_{we}^1 is the effective linear drag coefficient value. This relationship can be substituted directly for $\mathbf{V}_i$ used to determine the linear ice-water stress in terms of the true drag coefficient:

$$\boldsymbol{\tau}_w^1 = c_w^1 \mathbf{V}_i e^{i\beta} \tag{12}$$

where $\boldsymbol{\tau}_w^1$ is the ice-water stress computed using a linear drag law. So, substituting (11), the ice velocity computed using the effective drag values, into (12), the ice-water stress computed using the true drag coefficient and ice velocity, gives

$$\boldsymbol{\tau}_w^1 = c_w^1 \frac{\boldsymbol{\tau}_a^1}{f(\alpha^2 - 2\alpha \sin \beta + 1)^{1/2}} e^{-i(\delta - \beta)} \tag{13}$$

Inserting the values determined previously (Table 2) into (13) shows that the ice-water stress can be written directly in terms of the (linear) air-ice stress as

$$\boldsymbol{\tau}_w^1 \approx \frac{\boldsymbol{\tau}_a^1}{3} \tag{14}$$

Because the average $\delta - \beta$ angle is ~1.5°, the ice-water stress is essentially in the same direction as the air-ice stress (so the ocean drag on the ice is in the opposite direction). Note that the exact value of the denominator in (14) can be sensitive to the value of c_{we}^1, so if a variety of divergent/convergent conditions (and hence c_{we}^1 values) are anticipated, (13) should be used directly (equation (6) could be substituted directly into (13) for c_{we} as well).

Rule-of-Thumb Parameters

The simple proportionality between ice drift speed and wind speed, suggested by ignoring the Coriolis influence, is given by (3) and considered here. In general, since the effective $c_a \sim 0.75 c_w$, one might expect that for the thin Antarctic ice, the drift speed will be approximately $(0.75 \rho_a / \rho_w)^{-1/2}$, or ~3.0% of the wind speed at an angle equivalent to the average $\delta = 23.4°$. As above, the quality of this approximation is tested by comparing the predicted values of c_{rt}, using (3), to the optimal values determined numerically for each drift station. The rms error between observed drift and that predicted by this approximation is then compared with the rms error achieved using the quadratic form of the free drift equation.

The results of this test, summarized in Table 2 and Figures 11–13, show that the values of c_{rt}, predicted by (3), agree with the optimal fit values and that this simple rule-of-thumb formula consistently provides an excellent approximation to the quadratic free drift equation (using the average δ) and observations. In fact, as with the linear approximation, the rms errors are essentially indistinguishable from the quadratic formulation. Therefore the rule that the Antarctic ice drifts at ~3.0% of the wind speed at ~23°, appears justified. Specifically, applying (3) to the entire data set, using the overall effective value $c_w = 3.22 \times 10^{-3}$, yields an overall effective $c_{rt} = 0.0303 \pm 0.008$, $\delta = 23.4 \pm 1.3°$, this latter error reflecting the scatter in the optimal drift station fits.

5. SUMMARY

This paper uses the WWSP-86 winter Antarctic ocean, sea-ice, and meteorologic data to evaluate the appropriate-

ness of several useful formulations of the ice momentum balance equation and determine the relevant parameter values for these formulations. Table 2 and Figures 10–13 summarize many of our findings.

We find that the large-scale mean divergence of the winter sea-ice field justifies, with some penalty, use of the free drift equation, in which the force related to internal ice stresses is neglected explicitly. We considered three progressively simpler approximations of this formula: (1) the air-ice and ice-water stresses were parameterized using a quadratic drag law, a common parameterization which is essentially consistent with PBL theory and empirical evidence; (2) stresses were parameterized using a linear drag law, a convenient, analytically manageable form but less consistent with theory and observations; and (3) the Coriolis influence was neglected because of the thin sea-ice cover which results in a simple rule-of-thumb formula in which ice speed is proportional to wind speed.

Calculation of the optimum parameter values for each formulation and subsequent modeling of the ice drift using these values and formulations revealed that all three approximations simulate the observed ice drift to within the same accuracy, as measured by the rms error (see Table 2 and Figures 11–13). This indicates that the linear drag law, though weak theoretically, represents an excellent approximation to the quadratic drag law over a wide range of forcing. Antarctic modeling studies can take full advantage of the linear form without suffering ill effects. The rule-of-thumb formula was equally accurate in all cases considered and thus indicates the negligible role played by the Coriolis force as a result of the thin ice cover. It offers a quick, yet accurate, means of estimating the ice drift from knowledge of the wind velocity (ice drifts at ~3% of the wind speed, ~23° to its left).

Several important methodological considerations are clear from the analysis:

1. Direct inversion of the free drift equation for estimation of the quadratic drag law parameters requires robust regression techniques but still suffers from a skewed solution in the presence of noisy data because of the highly nonlinear nature of the regression variables with respect to the external variables. We found direct numerical optimization to be better.

2. Successful use of the linear drag law demands that both air-ice and ice-water stresses be written in terms of the linear law. If the quadratic law is used for the air-ice stress with a linear ice-water stress, the ice-water drag coefficient becomes a nonconstant function of wind speed, and use of a constant ice-water drag value will fail.

3. The linear drag coefficient values can be computed directly from knowledge of the quadratic drag coefficient values (most often published) using (7) for the air-ice stress and (7) or (10) for the ice-water stress. These estimates were shown to agree with the computed optimum values to ≲2%.

The optimum parameter values (drag coefficients, turning angles, and proportionality constants) for the various model formulations are presented with error estimates in Table 2. Because of the ~95% ice concentration prone to random ice bumping and evidence of convergence events (ice ridging, lack of inertial motion, and periodic decreases in large-scale ice surface area), the free drift formulation often forces an inflation of the ice-water drag coefficient values because the ice-ocean drag must effectively subsume the forces related to the gradients of internal ice stress. To isolate periods of true free drift, the 270 hours of ice drift measurements were divided into 6-hour segments (the minimum stable interval), and the ice-water drag coefficients and turning angles computed individually for each segment. The individual estimates were compared with evidence suggesting the degree of ice convergence/divergence in an effort to differentiate between estimates representing true free drift conditions and those in which ice interaction contributed a significant influence. Those estimates thought to represent periods of true free drift were combined to estimate the "true" or "pure" drag law parameter values (including the effects of form drag). These are $c_w = 1.62 \times 10^{-3}$ and $\beta = 15.2°$ (relative to the undisturbed ocean flow below the OBL). The average of the optimal parameter estimates from each of the three drift stations analyzed (similar to the median value of all 6-hour segment estimates) represents the overall "effective" quadratic drag law parameter values (i.e., inflated to account for typical levels of ice interaction). These are $c_w = 3.22 \times 10^{-3}$ and $\beta = 18.1°$. These "best" values are indicated by asterisks in Table 2.

The effective drag coefficient was shown to be highly correlated to the 4- to 5-day average large-scale ice divergence. The corresponding regression equation (6) predicts these drag coefficient values to within 5% of the optimal values. However, because of the limited data base used to predict the regression coefficients, further observations are required to reveal the true potential and limitations of this correlation. The effective values for the linear drag law and rule-of-thumb parameters were computed directly from (10) and (3) and given in Table 2.

Use of the effective drag coefficients allows a reasonable description of the pack ice movement and transfer of momentum from the atmosphere to the ice under typical Antarctic conditions. However, these effective values cannot be used to estimate the transfer of momentum from the atmosphere to the ocean through the ice, since their inflated size, representing unmodeled ice interaction, would be interpreted as increased ice-water stress driving the ocean. Instead, the effective values must be used to compute the ice velocity, which is then used to estimate the ice-water stress using the true drag coefficient values. Alternatively, the linear drag law allows the ice-water stress to be written directly in terms of the air-ice stress, giving $\tau_w^1 \approx (\tau_a^1)/3$ (see (12) and (13)) in the approximate direction of τ_a^1 (and in the opposite direction of the ice-water drag felt by the ice). So, in the presence of an ice cover subject to typical Antarctic conditions, the ice-ocean stress is ~1/3 the air-ice stress and in approximately the same direction. This relationship also reveals that the ice interaction does play a significant role in the Antarctic pack ice momentum balance and, while the free drift equation (with effective drag coefficient) represents an excellent parameterization of the ice drift itself, it does so at the cost of neglecting the details of the underlying physics.

The true quadratic drag law parameter values can be used in the momentum balance equation (1), in which the forces related to internal ice stresses are explicitly included. These values also allow estimation of the thickness of the inertial sublayer of the OBL. For ice drift velocities of ~30 cm/s (wind speeds of ~9 m/s), simple theory suggests that the inertial sublayer is 0.5–6 m thick and the surface roughness ≲4 mm, though direct PBL measurements are required to resolve this.

Finally, we note that the thin Antarctic seasonal sea-ice cover appears to be subject to a significantly lower ice-water drag than the thick multiyear Arctic ice. Measurements of thin first-year Arctic ice by *Langleben* [1982], though, show (quadratic) drag coefficients smaller than those estimated here. Our computed values, compared with the measured air-ice quadratic drag coefficient of 2.36×10^{-3} (15-m reference height), yield a ratio of $c_w/c_a \approx 0.75$ compared with values often >1 in the Arctic. The values and conclusions reported here apply to the open-ocean Antarctic pack ice away from the coastal regions and western Weddell Sea region, where multiyear ice and strong convergence may significantly influence ice drift.

Acknowledgments. We thank the crew and captain of the R/V *Polarstern* for field assistance, and S. Ackley, B. Burns, A. Omstedt, and M. McPhee for comments on the manuscript. D.G.M.'s work was supported by National Science Foundation research grant DPP 8501976. Lamont Doherty Geological Observatory contribution 4519 and Alfred-Wegener Institut für Polar und Meeresforschung contribution 192.

REFERENCES

Anderson, R. J., Wind stress measurements over rough ice during the 1984 Marginal Ice Zone Experiment, *J. Geophys. Res.*, *92*, 6933–6941, 1987.

Andreas, E. L., W. B. Tucker III, and S. F. Ackley, Atmospheric boundary layer modification, drag coefficient, and surface heat flux in the Antarctic marginal ice zone, *J. Geophys. Res.*, *89*, 649–661, 1984.

Brennecke, W., Die ozeanographischen Arbeiten der Deutschen Antarktischen Expedition 1911–1912, *Aus Arch. Deut. Seewarte*, *34*, 195, 1921.

Feldman, U., P. J. Howarth, and J. A. Davies, Estimating surface wind direction over drifting open pack ice, *J. Geophys. Res.*, *86*, 8117–8120, 1981.

Gordon, A. L., E. Molinelli, and T. Baker, Large-scale baroclinicity of the Southern Ocean, *J. Geophys. Res.*, *83*, 3023–3032, 1978.

Gordon, A. L., D. G. Martinson, and H. W. Taylor, The wind-driven circulation in the Weddell-Enderby Basin, *Deep Sea Res.*, *28A*, 151–163, 1981.

Guest, P. S., and K. L. Davidson, The effects of observed ice conditions on the drag coefficient in the summer east Greenland Sea marginal ice zone, *J. Geophys. Res.*, *92*, 6943–6954, 1987.

Hibler, W. D., III, Ice dynamics, in *The Geophysics of Sea-Ice*, edited by N. Untersteiner, pp. 577–640, Plenum, New York, 1986.

Hibler, W. D., III, and K. Bryan, Ocean circulation: Its effects on seasonal sea-ice simulation, *Science*, *224*, 489–491, 1984.

Hoeber, H., and M. Gube-Lehnhardt, The eastern Weddell Sea drifting data set of the Winter Weddell Sea Project (WWSP) 1986, *Ber. Polarforsch.*, *37*, 108 pp., 1987.

Langleben, M. P., Water drag coefficient of first-year sea ice, *J. Geophys. Res.*, *87*, 573–578, 1982.

McPhee, M. G., A simulation of inertial oscillation in drifting pack ice, *Dyn. Atmos. Oceans*, *2*, 107–122, 1978.

McPhee, M. G., The effect of the oceanic boundary layer on the mean drift of pack ice: Application of a simple model, *J. Phys. Oceanogr.*, *9*, 388–400, 1979.

McPhee, M. G., An analysis of pack ice drift in summer, in *Sea Ice Processes and Models*, edited by R. S. Pritchard, pp. 62–75, University of Washington Press, Seattle, 1980.

Menke, W., *Analysis of geophysical data: Discrete inverse theory*, 260 pp., Academic, San Diego, Calif., 1984.

Overland, J. E., Atmospheric boundary layer structure and drag coefficients over sea ice, *J. Geophys. Res.*, *90*, 9029–9049, 1985.

Pease, C. H., S. A. Salo, and J. E. Overland, Drag measurements for first-year sea ice over a shallow sea, *J. Geophys. Res.*, *88*, 2853–2862, 1983.

Rossby, C.-G., and R. B. Montgomery, The layer of frictional influence in wind and ocean currents, *Pap. Phys. Oceanogr. Meteorol.*, *3*, 1–100, 1935.

Rousseeuw, P. J., and A. M. Leroy, *Robust Regression and Outlier Detection*, 329 pp., John Wiley, New York, 1987.

Thorndike, A. S., and R. Colony, Sea ice motion in response to geostrophic winds, *J. Geophys. Res.*, *87*, 5845–5852, 1982.

Wadhams, P., M. A. Lange, and S. F. Ackley, The ice thickness distribution across the Atlantic sector of the Antarctic Ocean in midwinter, *J. Geophys. Res.*, *92*, 14,535–14,552, 1987.

D. G. Martinson, Lamont-Doherty Geological Observatory and Department of Geological Sciences, Columbia University, Palisades, NY 10964.

C. Wamser, Alfred-Wegener Institut für Polar und Meeresforschung, Am Handelshafen 12, 2850 Bremerhaven, Federal Republic of Germany.

(Received March 31, 1989;
accepted June 8, 1989.)